ELSEVIER

Tectonophysics 322 (2000) 163–190

TECTONOPHYSICS

www.elsevier.com/locate/tecto

Quantifying Precambrian crustal extraction: the root is the answer

Dallas Abbott [a,*], David Sparks [b], Claude Herzberg [c], Walter Mooney [d], Anatoly Nikishin [e], Yu Shen Zhang [f]

[a] *Lamont–Doherty Earth Observatory, Palisades, New York, NY 10964, USA*
[b] *Texas A and M, College Station, Texas, TX 77843, USA*
[c] *Rutgers University, New Brunswick, NJ 08903, USA*
[d] *US Geological Survey, Menlo Park, CA 94025, USA*
[e] *Geological Faculty, Moscow State University, Moscow 119899, Russia*
[f] *UC Santz Cruz, Santa Cruz, CA 95064, USA*

Received 7 June 1999; accepted for publication 19 October 1999

Abstract

We use two different methods to estimate the total amount of continental crust that was extracted by the end of the Archean and the Proterozoic. The first method uses the sum of the seismic thickness of the crust, the eroded thickness of the crust, and the trapped melt within the lithospheric root to estimate the total crustal volume. This summation method yields an average equivalent thickness of Archean crust of 49 ± 6 km and an average equivalent thickness of Proterozoic crust of 48 ± 9 km. Between 7 and 9% of this crust never reached the surface, but remained within the continental root as congealed, iron-rich komatiitic melt. The second method uses experimental models of melting, mantle xenolith compositions, and corrected lithospheric thickness to estimate the amount of crust extracted through time. This melt column method reveals that the average equivalent thickness of Archean crust was 65 ± 6 km, and the average equivalent thickness of Early Proterozoic crust was 60 ± 7 km. It is likely that some of this crust remained trapped within the lithospheric root. The discrepancy between the two estimates is attributed to uncertainties in estimates of the amount of trapped, congealed melt, overall crustal erosion, and crustal recycling. Overall, we find that between 29 and 45% of continental crust was extracted by the end of the Archean, most likely by 2.7 Ga. Between 51 and 79% of continental crust was extracted by the end of the Early Proterozoic, most likely by 1.8–2.0 Ga. Our results are most consistent with geochemical models that call upon moderate amounts of recycling of early extracted continental crust coupled with continuing crustal growth (e.g. McLennan, S.M., Taylor, S.R., 1982. Geochemical constraints on the growth of the continental crust. Journal of Geology, 90, 347–361; Veizer, J., Jansen, S.L., 1985. Basement and sedimentary recycling — 2: time dimension to global tectonics. Journal of Geology 93(6), 625–643). Trapped, congealed, iron-rich melt within the lithospheric root may represent some of the iron that is 'missing' from the lower crust. The lower crust within Archean cratons may also have an unexpectedly low iron content because it was extracted from more primitive, undepleted mantle.

Keywords: Archean; crust; growth rates; lithosphere; mantle; Precambrian; xenoliths

* Corresponding author.
E-mail address: dallas@ldeo.columbia.edu (D. Abbott)

0040-1951/00/$ - see front matter
PII: S0040-1951(00)00062-7

1. Introduction

One of the outstanding problems in understanding the evolution of the Earth's crust is determining the rate of continental growth over time. It is known that about 40% of the Earth's surface is covered by continental crust, which is best defined as an unsubductable layer of rocks and sediments (Abbott et al., 1997). Areas of pre-1.8 Ga crust have overall lithospheric thicknesses of 220–400 km, much thicker than the 120–150 km thick lithosphere in regions of post-1.8 Ga crust (Jordan, 1978, 1988; Lerner-Lam and Jordan, 1987; Nolet et al., 1994). In contrast, pre-1.8 Ga continental crust has (within error) the same thickness as post-1.8 Ga continental crust (Table 1). These similarities in crustal thickness juxtaposed with large differences in lithospheric thickness could arise because the crust was modified over time or because continental crust formed differently over time (Abbott and Hoffman, 1984; Martin, 1986).

The processes by which continental crust is initially formed are still debatable. There are basically two models: the island arc model and the oceanic plateau model (Condie, 1999). The island arc model for the origin of the continental crust states that new continents are formed at subduction zones by the partial melting of the mantle wedge above the subducting plate (and sometimes by the melting of the subducting plate itself) (Kay and Kay, 1986; Reymer and Schubert, 1986; Plank and Langmuir, 1988). Because much of the upper continental crust appears to have chemical characteristics similar to convergent zone magmas, this model goes far toward explaining the observed composition of much of the continental crust. It is clear that most continental crust is affected by arc volcanism during its evolution. The question

Table 1
Seismic thickness and volume of crust and lithospheric mantle in the region between 80°N and 80° S

Name	Minimum	Mean	Maximum
Archean crust			
Crustal thickness (km)	36.4	39.4	42.4
Surface area (10^6 km^2)	36.8	40.9	45.0
Total crustal volume (10^9 km^3)	1.3	1.6	1.9
Thickness depleted mantle (km)	197	203	209
Lithosphere volume (10^9 km^3)	7.3	8.3	9.4
Early Proterozoic			
Crustal thickness (km)	35.0	41.6	48.3
Surface area (10^6 km^2)	29.3	132.5	35.7
Total crustal volume (10^9 km^3)	1.0	1.4	1.7
Thickness depleted mangle (km)	188	196	204
Lithosphere volume (10^9 km^3)	5.5	6.4	7.3
Post-Early Proterozoic			
Crustal thickness (km)	30.3	37.1	43.9
Surface area (10^6 km^2)	78.4	87.1	95.8
Total crustal volume (10^9 km^3)	2.5	3.2	4.2
Thickness depleted mantle (km)	93	97	101
Lithosphere volume (10^9 km^3)	7.3	8.4	9.6
Total crust			
Total surface area (80N–80S)	144.4	160.4	176.4
Total crustal volume (10^9 km^3)	4.7	6.2	7.8
Volume mantle root (10^9 km^3)	20.1	23.1	26.3
Percentage volume upper mantle (crust)	0.5	0.7	0.9
Percentage volume upper mantle (root)	2.2	2.5	2.9
Percentage volume depleted upper mantle needed to make the crust	26.5	40.6	44.8

is whether or not arc volcanism (unaided by plumes) can extract sufficient melt from the mantle wedge to make enough unsubductable material to form the volume of continental crust that is observed.

The oceanic plateau model states that new continents are formed by high degrees of partial melting within mantle plumes(Abouchami et al., 1990; Boher et al., 1992; Stein and Goldstein, 1996). When they reach the Earth's surface, mantle plumes erupt large quantities of basaltic lava. In the ocean basins, these lavas form oceanic plateaus. When oceanic plateaus reach a subduction zone, some are too thick and too buoyant to subduct, and therefore, they become part of a continent (Abbott et al., 1997; Mann et al., 1997; Petterson et al., 1997). The magmatic processes at convergent margins, through processes of partial melting, fractional crystallization, magma mixing, and so forth, cause the observed composition of the crust to change to the more silicic compositions that appear at the surface.

At the current time, much of the data appears to favor the oceanic plateau model. Boninites, a type of magma that forms only where the overriding plate is both oceanic and hot (Pearce et al., 1992), are rare in the early Precambrian geological record (Abbott and Mooney, 1995; Wyman, 1999). If most early continental crust formed at island arcs, there should be many more recognized boninites. The continental crust also has too much Ni and Cr to be explained by the island arc model (Taylor and McLennan, 1985). A recent re-evaluation of the average composition of the continental crust shows that it is lower in K_2O (0.9%) than previously thought (Rudnick et al., 1998). This, too, favors the oceanic plateau model.

The observed episodicity of continental growth has been used as evidence for the oceanic plateau model (Abbott and Mooney, 1995; Stein and Goldstein, 1996). However, episodic continental growth can result from the increased seafloor spreading rates caused by superplumes (Larson, 1991), or it can result from the addition of unsubductable oceanic plateaus produced by plumes. In the former case, the increased spreading rates are accompanied by more rapid subduction rates, thereby increasing the rate of production of new island arcs. In the latter case, the continental crust grows in surface area and volume by the addition of plume-generated oceanic plateaus. Thus, episodic continental growth (Gurnis and Davies, 1986; Stein and Hofmann, 1994) is largely a result of superplume events. Superplumes may produce continental growth by a combination of plateau and arc addition.

Another observation that is difficult to explain is that oceanic plateau basalts are much richer in iron than average lower continental crust (Mahoney et al., 1992; Rudnick, 1992). Because the lower part of the continental crust has a basaltic composition (Christensen and Mooney, 1995; Rudnick and Fountain, 1995), it may represent relatively unmodified parts of an originally basaltic oceanic plateau. However, lower crustal xenoliths have average FeO contents of about 9% (Rudnick and Presper, 1990). This is much lower than the FeO content of Ontong Java plateau basalts (Mahoney et al., 1992), which are typically about 11% FeO. If continents are the result of plume volcanism, why is the lower continental crust not rich in iron? A reasonable model of continental growth must explain why the observed lower crust has so little iron (Rudnick, 1995).

It is possible that the low iron content of the lower continental crust may be the result of large quantities of unerupted, congealed komatiitic melt. Experimental data suggest that komatiitic melt could become too dense to rise into the upper levels of the mantle root (Herzberg et al., 1983; Agee and Walker, 1993; Ohtani et al., 1995). If so, iron-rich komatiitic melt might rise some distance from its source to a level of neutral density before becoming trapped within the lithospheric root. This melt would react with the surrounding mantle as it solidified. If such trapped, congealed melt had a sufficient volume, it might provide a complementary iron reservoir to the lower continental crust.

There are basically two types of geochemical models for the rate of growth of the continental crust.. The first is that of Armstrong (1981) and can be called the 'early growth/recycling' model. Armstrong (1981) proposed that the bulk of continental material was separated from the mantle early in the Earth's history and that subsequent apparent growth is the result of the recycling of pre-existing crust through erosion and reactivation. However, many others have proposed that the addition of new material to the continents has been continually occurring over the history of the Earth (e.g. McLennan and Taylor, 1982; Veizer and Jansen, 1985). In these 'steady growth' models, the growth of continental crust by the addition of new mantle-derived material began early in Earth history and is ongoing. The 'steady growth' model and the 'early growth/recycling' model each have profoundly different implications for the origin of cratons and lithospheric roots.

These two types of geochemical models are subject to direct tests by observations of the presently existing volume of early Precambrian continental crust. Any viable geochemical model of crustal growth must be able to produce, as a minimum product, the presently existing volume of early Precambrian crust. The earliest such measurements were those of Hurley and Rand (1969). They calculated the amount of continental crust of various ages based on the surface distribution of isotopic ages, and they assumed that there were no age-dependent differences in crustal thickness and density. One of the problems with the data of Hurley and Rand (1969) is that subsequent improvements in isotopic analyses and new mapping have shown that there is much more very old crust than they had known (Graham et al., 1999; Tucker et al., 1999).

In this paper, we attempt to constrain the minimum rate of continental growth over time by taking advantage of newer estimates of crustal thickness, crustal erosion, lithospheric thickness, lithospheric composition, and geochronology. We are particularly interested in estimating the amount of continental crust that was present by 2.4 Ga and by 1.8 Ga. We also show how the observed structure and composition of the continental crust and the lithospheric mantle could arise from accreted oceanic plateaus that were later modified by arc volcanism.

2. Assembling the essential databases

In order to constrain the minimum rate of continental growth, it was first necessary to compile and organize the data for each of the variables that we intended to use in our calculations. These variables include the distribution of crustal thickness, the age distribution of continental crust, the erosion level of the crust, and the estimated amount of trapped, congealed melt. It was also necessary to calculate the total volume of the lithospheric roots of the continents. The methods for compiling these data and the reasoning behind them are discussed in the following sections.

3. Estimating the thickness of the lithosphere

The lithospheric root represents the most depleted part of the residual mantle remaining after the crust had been extracted from the mantle. As the crust increased in volume, the volume of severely depleted lithospheric mantle also increased. Thus, the volume of this depleted residue is directly related to the amount of the crust that was extracted from the mantle at each time in Earth history. Because the oldest roots are so refractory and buoyant, they are very difficult to recycle into the convecting mantle As a result, the oldest lithospheric roots may remain beneath their original crust while the upper crust moves laterally due to erosion by streams, thrusting during compressional events and block faulting during extensional events. Consequently, the volume of the lithospheric root beneath cratons may contain a complementary record of the amount of crust that was extracted during early Earth history.

Because the volume of lithospheric roots is an indirect measure of the amount of crustal extraction, we need to estimate the thickness and lateral extent of continental lithospheric mantle. For the primary data set on lithospheric thickness, we used the S-wave, tomographic model of (Zhang and Tanimoto, 1991). This tomographic model has a nominal 5 by 5° resolution, but was resampled at a 2 by 2° resolution. We used horizontal slices through the model that were spaced at 20 km depth intervals. These slices were stacked on top of one another to derive a vertical cross-section of the Earth at a given point. Because the average velocity changes as a function of pressure, we worked with velocity anomalies rather than the absolute velocity.

The Zhang and Tanimoto model (Zhang and Tanimoto, 1991) is not corrected for the effect of asthenospheric temperature changes. Because the lithospheric mantle is chemically depleted in comparison with the surrounding asthenosphere, it has a different seismic velocity. However, the seismic velocity of the lithospheric mantle also changes as its temperature changes.

In a tomographic model that has not been corrected for temperature variations, a given anomaly in travel time will not correspond uniformly to a given degree of mantle depletion. That is, an uncorrected tomographic model will overestimate the thickness of the lithospheric mantle in areas where the surrounding asthenosphere is unusually cold, and it will underestimate the lithospheric thickness where the surrounding asthenosphere is unusually warm. Consequently, it was necessary to correct the model of Zhang and Tanimoto (1991). In order to do this, we had to estimate the variations in temperature in the asthenosphere.

4. Temperature variability in the asthenosphere

It is known that the asthenosphere at depth has large-scale lateral temperature variations. The problem has been to identify the relative contribution from shallow and deep temperature variations using techniques where all observation points are at the surface of the Earth. Recent seismic studies get around this problem by measuring the differential travel time between two seismic discontinuities (Gossler and Kind, 1996).

In the upper mantle, there are two major seismic discontinuities: one at approximately 410 km depth, and the second at approximately 660 km depth. These zones are called discontinuities because they have a large contrast in seismic velocities across them, and this sharp contrast in seismic velocities causes seismic energy to be reflected by them. The seismic energy that is reflected by both of these discontinuities is received at the same seismic station at slightly different times. The differences in travel times for seismic waves reflected from the two discontinuities are a measure of the temperature of the mantle(Liu, 1994; Gossler and Kind, 1996).

These discontinuities are caused by mineralogical phase changes in the mantle, but not all phase changes produce discontinuities. At roughly 410 km, olivine changes to its beta (higher pressure) form, wadsleyite, and at roughly 660 km, spinel olivine changes to Mg-perovskite. Both of these phase changes are strong reflectors of seismic energy and have been well-mapped. However, at about 500 km depth, beta olivine (wadsleyite) converts to the spinel form of olivine, ringwoodite. For unknown reasons, this phase change does not often produce an observable seismic discontinuity.

What is important for our purposes in this paper is that the exact depths of the olivine:beta olivine (circa 410 km) and spinel olivine:Mg-perovskite (circa 660 km) transitions are known to vary as a function of the temperature of the local mantle. Also, these two phase changes have different signs on their Clausius–Clapeyron slopes. That is, as the temperature decreases, the olivine:beta olivine transition occurs at a shallower depth and the olivine:Mg perovskite transition occurs at a deeper depth in the mantle. This is illustrated in Fig. 1. Thus, the variations in the travel times between the two discontinuities are due to both the variation in temperature and the increasing or decreasing distance between the discontinuities as a result of these variations in temperature. The correction for travel time variations due to the temperature of the lithospheric mantle is very small, only about 15% (Revenaugh and Jordan, 1991). Therefore, the bulk of the variation in travel time is the result of the differential movement of the two discontinuities (Fig. 1).

Overall, the temperature in the transition zone between the olivine:beta olivine (circa 410 km) and spinel olivine:Mg-perovskite (circa 660 km) transitions is estimated by Gossler and Kind (1996) to vary by about 200°C. This is a significant difference, but as stated above, the change in seismic velocity due to this temperature variation is small. However, the variation in temperature causes the relative depths of the seismic discontinuities to shift, so that the seismic energy must travel either a shorter or a longer distance between the discontinuities. It is this change in the depths of the

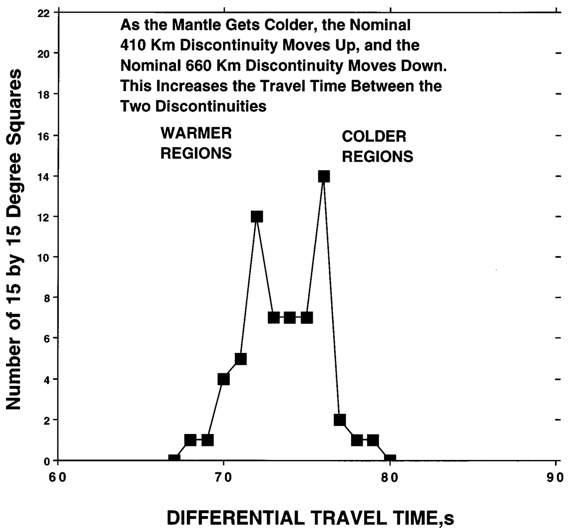

Fig. 1. Histogram of the travel time (in seconds) between the two major seismic discontinuities in the upper mantle. Both discontinuities are caused by phase changes in olivine. The phase changes cause a change in seismic velocity that results in an observable reflection of seismic waves. The travel time between the two discontinuities is a differential travel time derived by subtracting the arrival time of seismic energy reflected from the lower discontinuity from the arrival time of seismic energy reflected from the upper discontinuity. The differential travel times are from averages of data from 15 by 15° squares on the Earth.

discontinuities that causes almost all of the observed variations in the travel times between the two discontinuities.

Because lithospheric roots are highly depleted, their S-wave velocities are faster than those of comparable, undepleted mantle. The velocity changes are quite small, on the order of +0.5% (Jordan, 1978). Thus, they are in the same range as the velocity changes that are produced by temperature changes. We wish to correct for the effect of lateral temperature changes by finding some depth where there are no detectable velocity effects from lithospheric roots. However, the depth extent of lithospheric roots is debatable. Geochemists who study mantle xenoliths argue that they have a maximum thickness of only about 200 km (Boyd, 1987; Pearson et al., 1995b). Geophysicists who make tomographic models find that lithospheric roots go down to nearly 400 km depth (Grand, 1986; Lerner-Lam and Jordan, 1987). As a result, we needed to determine the maximum reasonable depth for lithospheric roots. We did this by looking at the correlation of slow seismic velocity anomalies with cratonic regions in successively deeper horizontal slices of the tomographic model. Once we reached a depth (350 km) where the slow seismic velocity anomalies were randomly correlated with cratonic regions, we concluded that we were below the lithospheric roots. Velocity anomalies at that depth are mainly the result of mantle temperature variations.

5. Correcting for lateral temperature variations

We used the velocity variations at 350 km depth as a proxy for temperature variations in the mantle. The velocity variations at 350 km depth have a relatively long wavelength. In order to calculate the variations in asthenospheric temperature, we must make two assumptions about the temperature structure of the mantle. Firstly, we assume that the lithospheric root is responsive to temperature changes in the underlying asthenosphere and that those temperature changes are observable by examining the velocity variations in the asthenospheric mantle. Secondly, we assume that heat transfer within the root involves linear thermal gradients (Rudnick et al., 1998).

The inferred horizontal length scale of variations in mantle temperature is quite broad, with average wavelengths of 1000–2000 km. This means that the overlying plate has millions of years to equilibrate its temperature profile with that of the underlying asthenosphere. The rate of heat transfer by conduction is on the order of 50 km in 10 Ma, equivalent to a plate tectonic velocity of 0.5 cm/yr. Continents typically move at velocities of 1–2 cm/yr (Stoddard and Abbott, 1996). However, radiative heat transfer goes as the absolute temperature to the fourth power, so there will also be a significant radiative component of heat transfer within the upper mantle. A recent re-evaluation of the temperature gradients within cratonic roots using improved geothermometry and geobarometry revealed linear, rather than curved, temperature–depth profiles (Rudnick et al., 1998; R. Rudnick, pers. commun.). If cratonic mantle roots were not in thermal equilibrium with the surrounding mantle, we would expect to find curved temperature–depth profiles using mantle xenoliths. This is not observed. Therefore, it is reasonable to assume that mantle roots are in thermal equilibrium with their surrounding asthenosphere.

To make the temperature corrections, the corrected tomographic model was merged into one file containing the vertical profiles of seismic velocity and of the velocity anomalies between 90 and 350 km depth. As explained above, we used the seismic data from the 350 km depth (the apparent maximum depth of compositional anomalies) as an index of the temperature of the asthenosphere. Then, we generated two sets of files: one in which the velocity data were not corrected for asthenospheric temperature variations, and one in which the data were corrected. The correction for the temperature of the asthenosphere was a linear conductive propagation of the velocity deviation at 350 km depth. We assumed that heat transfer between the asthenosphere and the overriding lithosphere produces linear variations in velocity anomalies with depth. That is, if the velocity deviation was $+1\%$ at 350 km depth, the velocity anomaly at 330 km was corrected downward by a quantity equal to $0.01 \times (330/350)$. Correspondingly, the velocity anomaly at 310 km was corrected downward by a quantity equal to $0.01 \times (310/350)$. We then used this result to correct the seismic velocities.

6. Computing the lithospheric thickness

We actually generated two models for lithospheric thickness: one using the uncorrected tomographic model of (Zhang and Tanimoto) 1991, and the other using the same tomographic model with corrections for lateral variations in asthenospheric temperature. Starting at 90 km depth, the calculation software is programmed to move down the velocity profile in a given tomographic slice of lithospheric mantle to a depth of 350 km. When the calculation reaches a depth where the measured seismic velocity is found to be less than $+1.005\%$ of the computed mean velocity of the Earth at that depth, that depth is registered as the lithospheric thickness for that slice. Because some lithosphere has seismic velocities between $+0.5\%$ and $+1.005\%$ of the mean velocity, our calculations provide a minimum estimate of lithospheric thickness. However, due to probable errors in the tomographic model, we decided to choose a conservative cut-off velocity between lithosphere and asthenosphere.

The results of the calculations using the uncorrected tomographic model are shown in Fig. 2a. The uncorrected tomographic model has a distribution of lithospheric thickness that is strongly bimodal between the continents and the ocean basins. Although some bimodality is expected, the uncorrected tomographic model shows too much thick lithosphere compared to what is known to exist from other studies. Furthermore, the uncorrected model shows an area of extremely thick lithosphere north of Australia that is partially due to subduction of buoyant continental lithosphere into the cold mantle beneath old, thick oceanic crust. Strictly speaking, this area does have a thick lithosphere, but the thickness of the continental lithosphere is overestimated.

The calculations using the corrected tomographic model produced much better results (Fig. 2b), although there are some lateral shifts in the location of thick lithosphere that we believe can be corrected with the better models that will eventually become available. Fig. 2b shows that the subduction zone artifact north of Australia is no longer present, and that the cratons in areas of recent hot spot activity in Africa and South America have a better resolution. Nevertheless, Africa and South America are much more poorly resolved compared to North America and Eurasia because there are fewer ray paths in Africa and South America. On average, the southern hemisphere has about half the number of ray paths of the northern hemisphere.

7. Comparing tomographic lithospheric thickness with a tectonic map

As a check on the results obtained with the corrected tomographic model (Fig. 2b), we made a tectonic map of lithospheric thickness (Fig. 3a). We used the following tectonic indicators of litha)

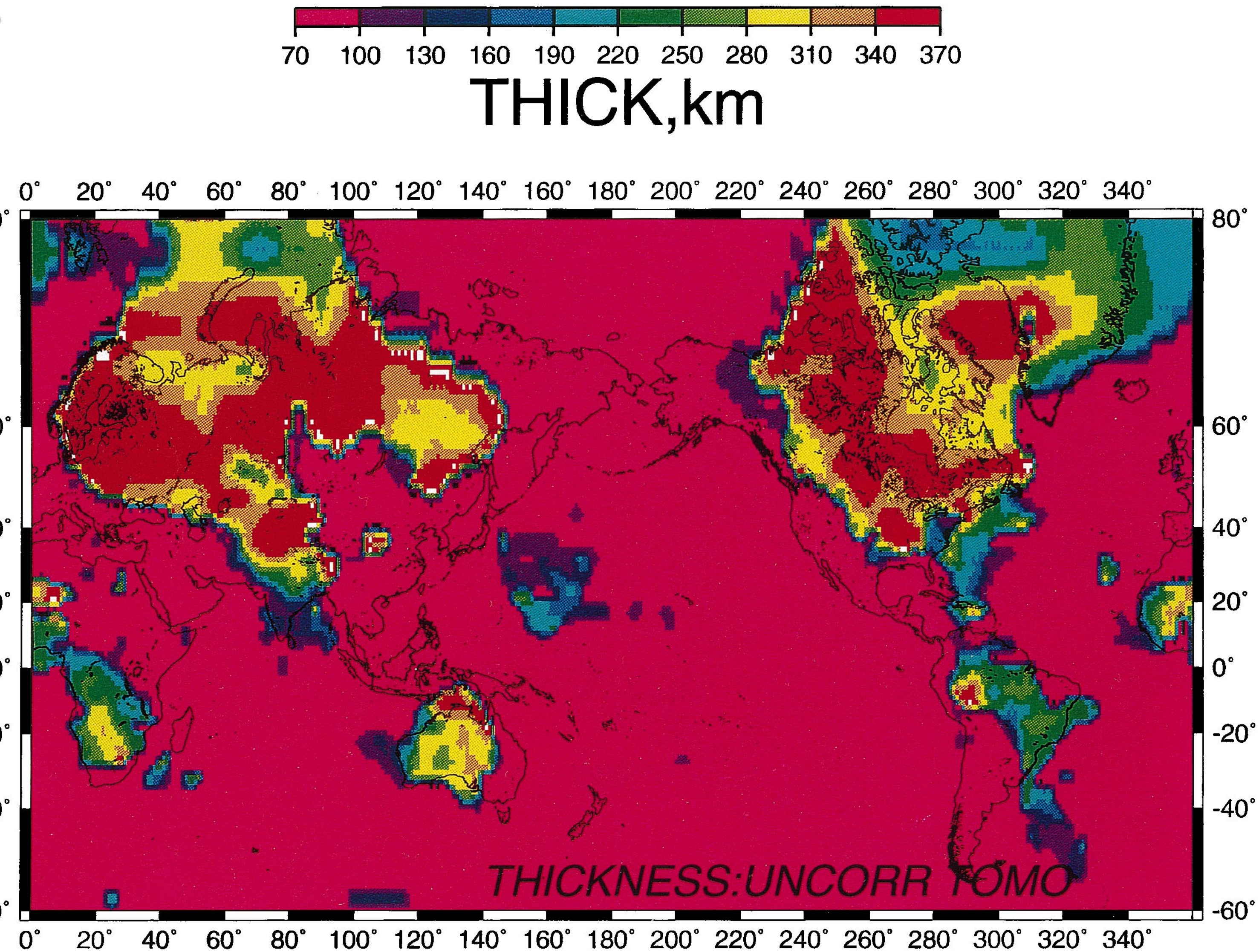
70 100 130 160 190 220 250 280 310 340 370
THICK,km
0° 20° 40° 60° 80° 100° 120° 140° 160° 180° 200° 220° 240° 260° 280° 300° 320° 340°
80° 60° 40° 20° 0° -20° -40° -60°
THICKNESS:UNCORR TOMO

b)

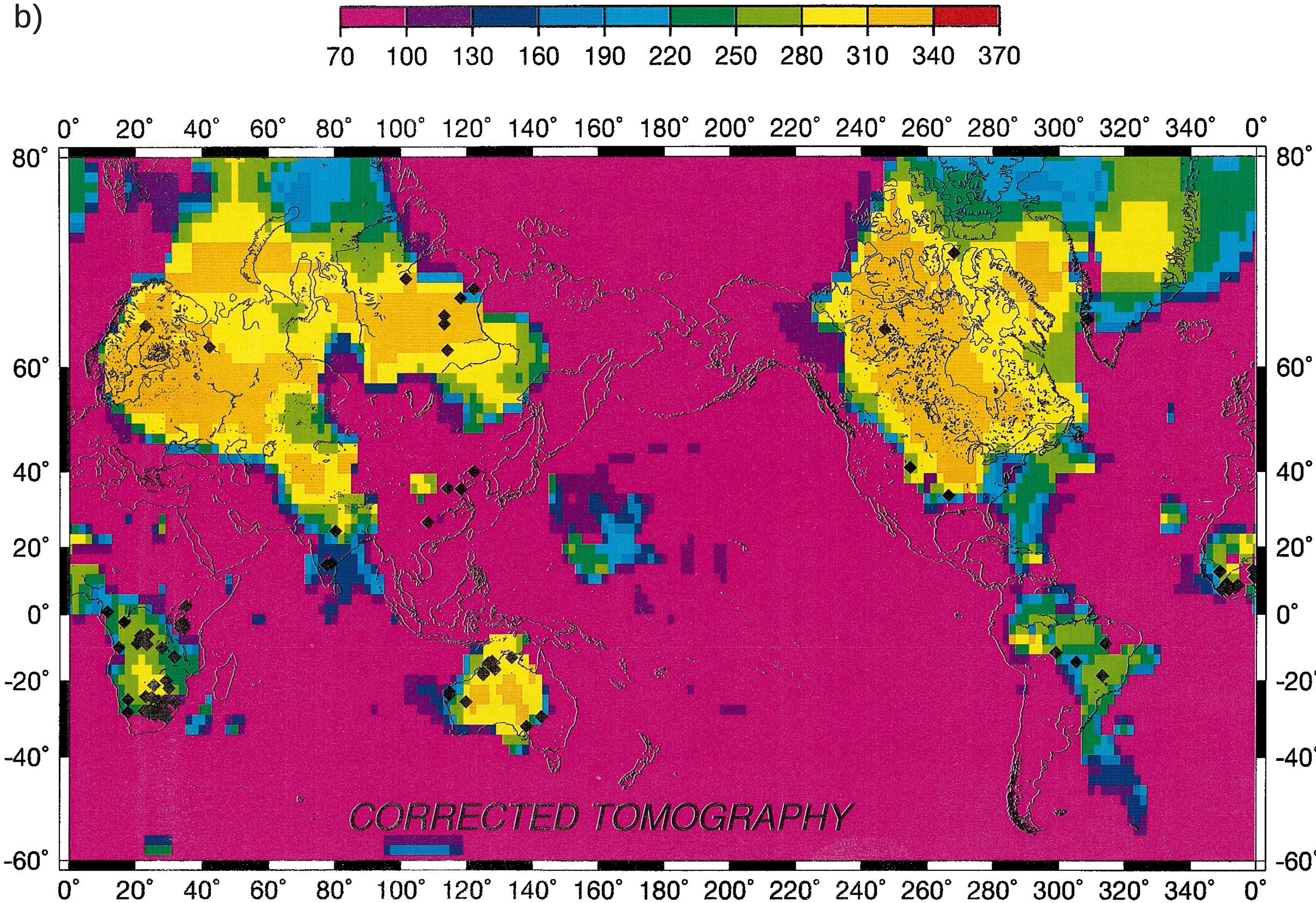

Fig. 2. (a) Global lithospheric thickness from a tomographic model that has not been corrected for temperature variations in the asthenosphere. The tomographic model has a typical resolution of 5 by 5°, but can be as poor as 8 by 8°. (b) Global lithospheric thickness from a corrected tomographic model. The tomographic model has a typical resolution of 5 by 5°, but can be as poor as 8 by 8°. Areas of thick lithosphere (>250 km) correspond broadly to cratonic areas. The resolution of the model is better in the northern hemisphere, where there are about twice as many ray paths. Areas of known diamondiferous kimberlites and lamproites appear as black diamonds.

a)

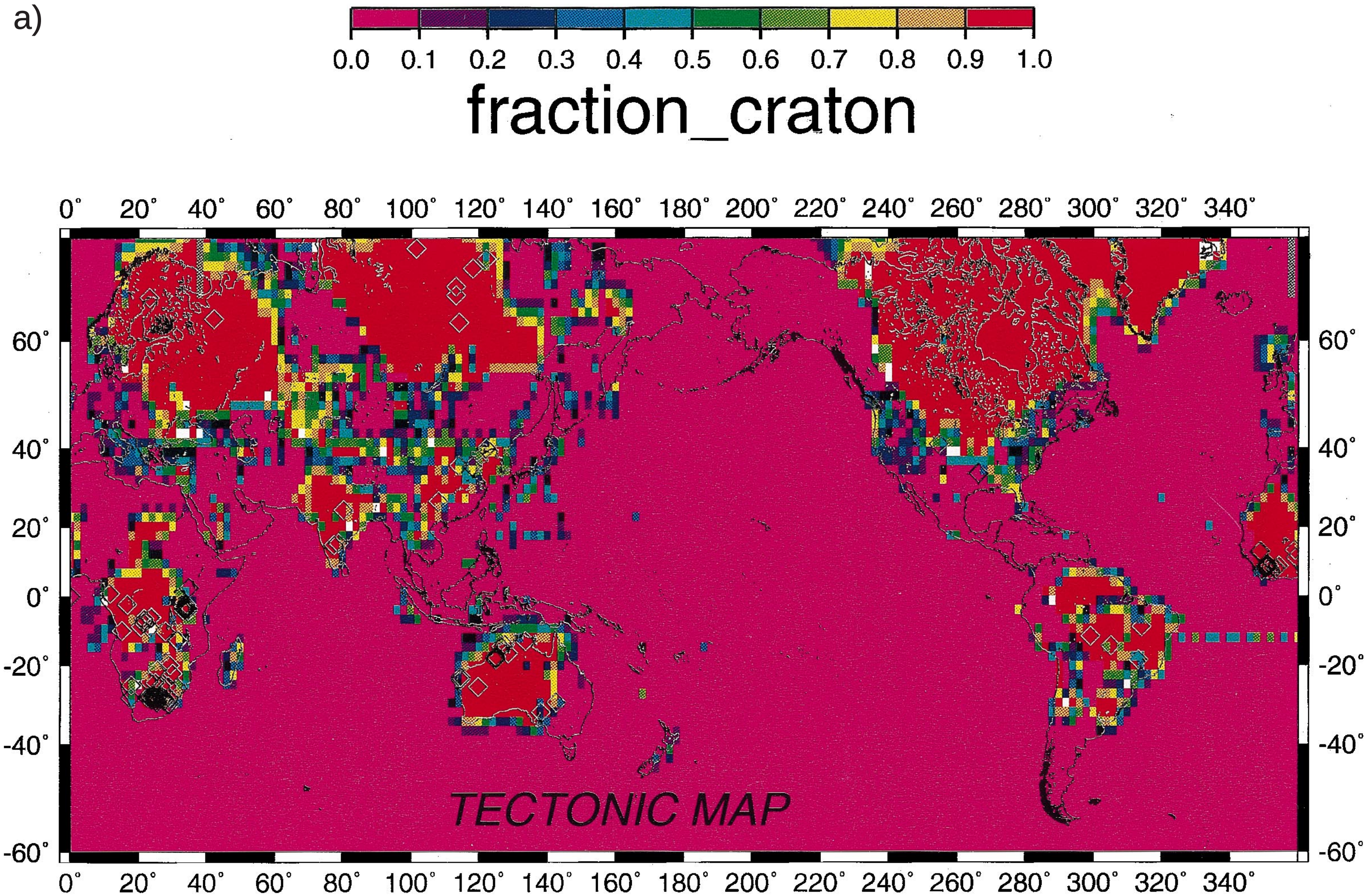
0.0 0.1 0.2 0.3 0.4 0.5 0.6 0.7 0.8 0.9 1.0
fraction_craton
0° 20° 40° 60° 80° 100° 120° 140° 160° 180° 200° 220° 240° 260° 280° 300° 320° 340°
60° 40° 20° 0° -20° -40° -60°
TECTONIC MAP

(b)

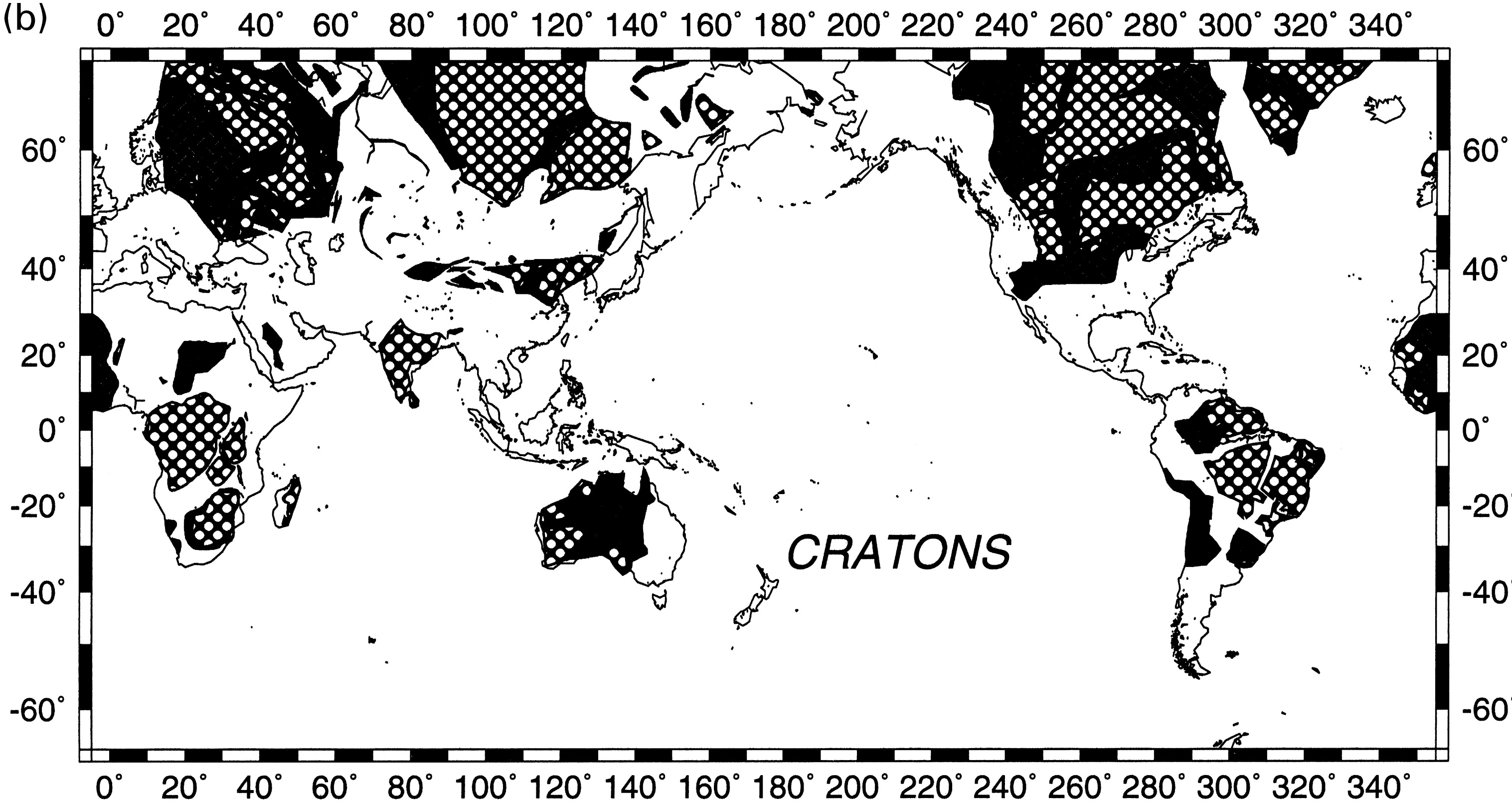

Fig. 3. (a) Fraction cratonic from cratonic indicators (age >1.8 Ga and heat flow <35 mW/m^2) and off craton indicators (age <1.8 Ga, heat flow >80 mW/m^2, and presence of basaltic volcanism). The data are averaged at a 2° grid spacing. Note that southern India and southern South America have cratonic areas that show up in this map that are poorly resolved in the tomographic model. Note also that the Madagascar shield is not well resolved on this map, due to the smoothing produced by a 2° grid spacing. Areas of known diamondiferous kimberlites and lamproites appear as white and black diamonds, respectively. (b) Estimated extent of Archean (black with white dots) and Early Proterozoic (black) continental crust.

ospheric thickness: heat flow, basement age, recent volcanism, and diamondiferous kimberlites or lamproites. Low heat flow and diamondiferous pipes are known to be characteristics of thick, cratonic lithosphere. Diamonds are not stable unless the lithospheric mantle is at least 150 km thick (Kennedy and Kennedy, 1969). Assuming average cratonic geotherms, the presence of diamondiferous mantle xenoliths is an indication that the underlying lithosphere is at least 175 km thick (Richter, 1988). Conversely, high heat flow, recent volcanism, and ages less than 1.8 Ga are usually correlated with lithosphere that is less than 150 km thick (Nixon, 1987; Nyblade and Pollack, 1993). The exceptions to these rules are some Archean areas that have had their thick lithosphere removed, for example, much of the Archean basement in China (Menzies et al., 1998).

The heat flow was derived from a database of reliable heat flow measurements, that is those from bore holes that are more than 100 m deep (Nyblade and Pollack, 1993). Because there are so few heat flow measurements within cratons, a simple gridding and smoothing of the data would bias the heat flow mean towards higher values.

For this reason, we divided the heat flow database into three groups: Archean (>2.4 Ga), early Proterozoic (1.8–2.4 Ga) and post-early Proterozoic (post-1.8 Ga) (Fig. 3b).

To prevent interpolation across craton boundaries, the boundaries of Archean and early Proterozoic cratons were assumed to have a heat flow value equal to the mean heat flow of these cratons. Where Archean and early Proterozoic cratons shared boundaries, they were assumed to have Archean values. The heat flow measurements were also truncated at values below 18 mW/m^2 (our estimated value of continental reduced heat flow) and above 250 mW/m^2 (estimated value of heat flow on 1 m.y. old crust) (Menke and Levin, 1994). These truncated heat flow values plus all reliable heat flow values were averaged within 1° squares. A smooth surface (GMT surface) was adjusted to fit the heat flow data exactly and to fill in all areas with no data.

After generating the heat-flow data set, we had two global data sets averaged over 1° blocks: basement age and heat flow. To make the tectonic map, we converted the two sets of gridded files (raster files) into ASCII files of points (lat, lon, value). We then assigned each set of points a value of 1 or zero based on the following strategy. If the area had a basement age greater than 1.8 Ga, it was given a a value of 1. If the area was younger, it was given a value of zero. In addition, areas of recent volcanic activity, heat flow higher than 80 mW/m^2, and mantle xenoliths erupted in alkali basalt were given a value of zero. Areas of heat flow less than 35 mW/m^2 were given a value of 1.

The ones and zeros were then averaged at a 2° grid spacing, like the tomographic model (Fig. 4). Two degree squares that have mean values of 0.9–1.0 plot as red, and are inferred to be cratonic. Two degree squares that have mean values of 0.0–0.1 plot as pink and are inferred to be non-cratonic. Areas with values of 0.9–0.1 are largely confined to craton boundaries.

When the tectonic map is compared with the tomographic map (Figs. 2b and 3b), we can evaluate the strengths and limitations of both methods

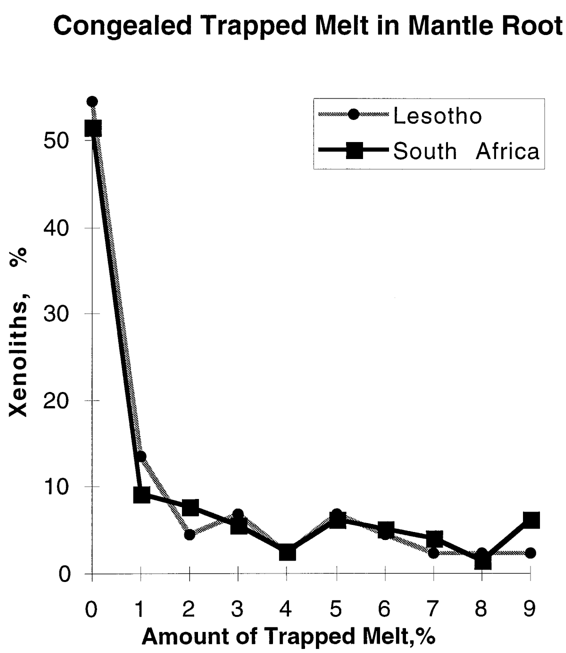

Fig. 4. Histograms of distribution of trapped, congealed melt in Archean (Kaapvaal) and Early Proterozoic (Lesotho) lithospheric mantle. As it cooled, this melt reacted with the surrounding, highly depleted mantle root.

for estimating lithospheric thickness. Remember that although the tomographic model was interpolated and resampled at a 2° grid spacing, the actual resolution of the tomographic model is just 5 by 5° in areas with larger numbers of ray paths. In areas with smaller numbers of ray paths (mostly in the southern hemisphere), the resolution is poorer, about 8 by 8°. In contrast, the tectonic map has a true 2° resolution. Thus, for the most part, the tectonic map is clearer, for example, in southern India. At the 5 by 5° resolution of the tomographic map, southern India would not appear as cratonic. On the tectonic map, southern India appears as cratonic because of a spatially restricted area of low heat flow ($<35\ mW/m^2$) surrounding two areas with diamondiferous kimberlites (Nixon, 1987). For this reason, we infer that southern India has not lost its cratonic root. We attribute the fact that the tomographic model does not show the presence of this thick lithosphere to poor resolution in the mantle tomography of this area. The tomographic model does show a broad area of slightly thickened lithosphere that appears to surround India. We believe that this broad area is an artifact of the smearing of the data in the tomographic model due to its averaging of seismic travel times within 5 by 5° squares.

The limited resolution of the tomographic model also explains why some known narrow cratonic areas do not appear on the tomographic map. In general, most of the cratonic blocks in the southern hemisphere have a much smaller lateral extent than the cratonic blocks in the northern hemisphere. Because the southern hemisphere cratons are usually smaller, and because the tomographic model uses fewer rays in the southern hemisphere, the overall resolution of the southern hemisphere is much poorer in the tomographic model than in the tectonic model. The only exception to this is Australia, which is well resolved in the tomographic model. For example, at the 2° grid spacing on the tectonic map, the Archean/Early Proterozoic craton of Madagascar (Agrawal et al., 1992; Handke et al., 1997; Rambelson, 1998) appears as intermediate thickness lithosphere (Fig. 4). In other words, although the starting model contained the cratonic area in Madagascar, the 2° gridding interval averaged it with adjacent, non-cratonic crust. Because the Madagascar craton is only a few degrees wide, Madagascar lost its definition as a cratonic area. In South America, the tectonic map shows that the southernmost cratonic area constitutes a block of four separate 2 by 2° squares (Fig. 3a). In a tomographic model with an 8 by 8° resolution, these blocks would disappear.

8. Geological implications of the tomographic results

Although the tomographic results are uneven in quality, and there is some smearing due to the grid spacing of the model, Fig. 3a shows that the areas of thick lithosphere shown in the tomographic model correspond broadly to the areas of thick lithosphere that are known to exist. For example, the Kaapvaal craton (in Southern Africa), the Canadian shield, the east European platform, the Kenema-Man shield (in West Africa) and the Siberian craton all have inferred maximum thicknesses in excess of 250 km. All of these areas are clearly shown on the tomographic map.

The tomographic results also confirm what had been previously inferred from studies of mantle xenoliths and heat flow distributions. The lithospheric root has been removed in Wyoming (Eggler and Furlong, 1991) and in eastern China (Nixon, 1987; Nyblade and Pollack, 1993), where only relatively old diamondiferous kimberlites are found. The lithospheric root is still present is many areas where younger diamondiferous kimberlites are found, in Saskatchewan, at Prairie Creek, Arkansas, in the Slave Province, at Akhangelsk, northern Russia, in Siberia, on the Kaapvaal craton, on the west African craton, on the Kimberly craton, and in north central Australia (Nixon, 1987; Menzies et al., 1993; Lambert et al., 1995; Pearson et al., 1995a,b; Griffin et al., 1999). The tomographic results also show evidence of thick lithospheric roots in areas where placer diamonds are found, but the source kimberlites have not been located: in the Ukrainian shield region, in the Hoggar region of Africa (22N, 5E) and in the southern Urals (56N, 59E) (Bardet, 1973, 1974; Nixon, 1987).

The tomographic model also shows some unexpected results that are confirmed by more recent work. Fig. 3a shows that the largest area of thick lithosphere within the ocean basins is east of the Mariana–Izu–Bonin arc, in the western Pacific. Given the resolution of the model, this corresponds in part to the Ogasawara plateau. The Ogasawara plateau contains thickened crust whose origin is not known (Smoot and Richardson, 1988). The tomographic model also shows thick lithosphere in the model extending well south of the Ogasawara plateau to the area just east of the Mariana arc. Analyses of peridotites dredged from the Mariana forearc produced Re/Os model ages of 0.8–1.1 Ga (Parkinson et al., 1998). The old model ages may result from the incorporation of older depleted mantle into younger (Mesozoic) seamount magmas in the Pacific. The tomographic model also shows a small area of thickened lithosphere around the Seychelles islands, midway between India and Madagascar. The Seychelles islands have Precambrian granites (Yanagi et al., 1983). Plate reconstructions show that the Seychelles islands are continental fragments that remained behind when India was rifted from Madagascar. Thus, it is reasonable to conclude that the Seychelles might have thick lithospheric mantle beneath them.

9. Calculating the present-day volume of the continental crust and lithosphere

In order to calculate the volume of the continental crust and lithosphere at particular times in the past, it is necessary first to calculate the volumes of the continental lithosphere, lithospheric mantle, and continental crust that exist at the present time. We used a map of 1° squares of the surface of the Earth between 80°N and 80° S. Each 1° square was assigned to an age range based on the predominant age of the crust within the square. The age categories were: 0–1.8 Ga, 1.8–2.4 Ga, and pre-2.4 Ga (Stoddard and Abbott, 1996). We have updated this map using more recent estimates of crustal age in Northern Eurasia (Abbott and Nikishin, unpublished manuscript). Using spherical trigonometry, the surface area of each square was calculated from its average width measured in longitude and height measured in latitude. We derived the crustal thickness by sampling the global 5° grid of crustal thickness (Mooney et al., 1998) at the grid point closest to the center of each 1° square. The present-day crustal volume for each age group was calculated by summing the surface area for that age group and multiplying the total surface area by the mean crustal thickness for that age group. The standard error of the crustal thickness was subtracted or added to the mean crustal thickness to derive the probable range of crustal thicknesses in each age group. The minimum and maximum values of the crustal volume for each age group used the surface areas multiplied by the minimum and maximum values of the crustal thickness for that age group (Table 1).

The overall lithospheric thickness is derived by merging our 1° crustal thickness grid with the nearest point in the tomographic model. The tomographic velocity anomalies were calculated for 5 by 5° boxes and then resampled at a 2° grid spacing. The two grids are different in scale, and there are some Archean and Early Proterozoic blocks that are too small to be resolved by the tomographic model. These small blocks represent less than 9% of the overall surface area of Archean and Early Proterozoic crust, a small fraction of the total. Therefore, we did not introduce any large errors by using the average lithospheric thickness of the larger blocks as the average lithospheric thickness of all Archean and Early Proterozoic blocks. Then, we calculated the lithospheric volume by multiplying the average lithospheric thickness in each age range by the total surface area covered by continental crust within that age range (Table 1).

The mantle root is the most depleted part of the lithospheric mantle that was melted to make the crust. This part of the mantle was so intensely depleted by melting and its physical properties so profoundly changed, that it became isolated from the asthenosphere. This means that the average thickness of the mantle root supplies a conservative or minimum estimate of the volume of mantle that was depleted by extraction of the continental crust. We calculated the average thickness of the mantle root, T_r

$$T_r = \frac{\sum_i (T_l - T_c)_i * (SA_i)}{SA_{total}}$$

where T_l is the average lithospheric thickness of one region i, T_c is the average crustal thickness of one region i, SA_i is the surface area of one region i and SA_{total} is the total surface area of all regions of that age. We used the standard errors in average crustal and lithospheric thicknesses to derive estimates of the maximum and minimum thicknesses of the mantle root (Table 1).

10. Change in crustal volume through time: summation method

The crustal volume at any given time in Earth history is equal to the total volume of different parts of the crust: the volume of the surficial crust, the volume of trapped (i.e. unerupted) melt, and the volume of previously eroded crust. The volume of the surficial crust is equal to the surface area of the crust multiplied by the seismically determined crustal thickness. This is equal to the thickness of continental crust above a prominent seismic reflector, the Moho. Ideally, we would prefer to use the petrological thickness of the crust, that is, the total thickness of material that is geochemically and mineralogically continental crust rather than lithospheric mantle. Although, in some areas, the geochemical crustal thickness is not the same as the geophysical crustal thickness (Griffin and O'Reilly, 1987), in most cratonic areas, the two thicknesses are the same. One problem with this statement is that seismologists cannot distinguish between olivine cumulates derived from crystallizing komatiitic melts and olivine residues comprising the depleted lithospheric mantle (Durrheim and Mooney, 1991). If such olivine cumulates exist, it is not possible to account for them.

We determine the volume of crust that has been eroded by using recent estimates of the metamorphic grade of undeformed Archean granite-greenstone terranes (Galer and Metzger, 1998). The mean burial pressure of 1.5 ± 0.5 km corresponds to a mean depth of erosion of 5 ± 2 km since 3.0 Ga. We use the standard error of the mean depth of erosion to obtain a minimum depth of erosion of 3 km since 3.0 Ga. The maximum burial pressure of 3 ± 1 kb corresponds to a maximum depth of erosion of 10 ± 3 kb since 3.0 Ga. We use these numbers to calculate the minimum, average and maximum erosional levels of recent, Proterozoic, and Archean crust.

Although much erosion results from horizontal compression and deformation of terranes, thermal changes in the Earth's mantle also cause long-term uplift of terranes. This uplift is related to changes in the isostatic balance between the depleted mantle root underneath continents and the asthenosphere beneath the mantle root (Galer, 1991). As the asthenospheric temperature declined over time, the depleted mantle roots became relatively more buoyant. The increased buoyancy of their mantle roots produced uplift and erosion of the continental crust. Our models of erosion of the continental crust consider only the erosion due to isostatic uplift produced by the long-term decrease in the average temperature of the Earth's mantle (Abbott et al., 1994).

Because erosion due to isostatic uplift is produced by temperature changes in the Earth's mantle, it must change as the internal heat production of the Earth changes (Galer, 1991). Because the internal heat production of the Earth decays exponentially over time (Wasserburg et al., 1964), we argue that mantle temperatures must decay exponentially over time (Abbott et al., 1994). [The present data set of mantle temperatures over time is too sparse and could be fit equally well by a model of linearly decreasing mantle temperatures over time (Galer, 1991; Galer and Metzger, 1998).] However, if mantle temperatures do fall exponentially as the Earth ages, the total thickness of the layer of eroded crust must also decrease exponentially over time. We have made three best-fit exponentially decaying models for the total thickness of eroded continental crust versus time:

$$E_{min} = \exp(A \times 0.462098) - 1.0$$

$$E_{av} = \exp(A \times 0.597253) - 1.0$$

$$E_{max} = \exp(A \times 0.799298) - 1.0$$

where E_{min}, E_{av} and E_{max} are the minimum, average and maximum estimates of the thickness of eroded crust in kilometers, respectively, and A is the age of the Earth in Ga (10^9 years). At 3.0 Ga, these equations yield a total thickness of eroded crust of 3, 5 and 10 km, respectively. We then used these equations to calculate the minimum, average and mean thickness of crust eroded from continental areas with Archean, Early Proterozoic and post-Early Proterozoic ages. The results are shown in Table 2.

11. Volume of trapped, solidified melt

In addition to the existing surface volume of the crust and the amount of crust that has been eroded and removed, we must also take into account the amount of melt derived from depleted mantle that was never erupted. That is, there is some crustal material that was never successfully transported above the depleted mantle in the lithospheric root. It remained trapped at depth where it would have congealed and reacted with the surrounding lithospheric root (Ireland et al., 1994). Because this trapped melt caused depletion of the mantle from which it was removed and therefore represents a petrological complement to depleted mantle, it must be included in any calculation of the mass balance of the volume of continental crust.

We calculated an estimate of the volume of trapped melt using the composition of xenoliths from South Africa and Lesotho. Both sets of xenoliths were found in the Archean age basement of the Kaapvaal craton. Our modeling procedure relies upon having large numbers of xenoliths (>50) with whole rock compositions that are all from a single cratonic region. For this reason, only the xenolith suites from South Africa and Lesotho are suitable for this type of modeling calculation.

The oldest rocks on the Kaapvaal craton with an extensive surface exposure are about 3.5 Ga (de Wit and Armstrong, 1987; Riganti and Wilson, 1995) The craton was stabilized at about 3.1 Ga (de Wit et al., 1992). Lesotho lies at the southern edge of the Kaapvaal craton, and part of the lithospheric mantle beneath Lesotho is early Proterozoic in age (Olive and Ellam, 1997). Therefore, we use the xenoliths from South Africa as proxies for the amount of trapped melt beneath Archean basement and the xenoliths from Lesotho as proxies for the amount of trapped melt beneath early Proterozoic basement.

We model the compositions of melts formed in a one-dimensional melting column, using a parameterization of deep melting experiments(Herzberg et al., 1983; Herzberg and Hara, 1998; Herzberg, 1999). The melts are assumed to mix completely, so the melt composition reflects melts formed over a range of depths. The residual mantle composition at any depth in the melting column is found by subtracting the composition of the pooled melts from all greater depths in the column, from the initial mantle, taken to be represented by KLB-1. Because mantle xenoliths are enriched in incompatible elements by kimberlitic magmas, we perform our modeling using only five major elements: Si, Al, Ca, Mg and Fe. These elements represent over 98% of most mantle peridotites (O'Neill and Palme, 1988) This strategy avoids the problem of contamination of the xenolith by the kimberlite magma.

The compositions of the pooled melt and residual mantle are controlled by the final depth of the residual mantle and the depth of initial melting (determined by mantle potential temperature). The compositions of a xenolith would also depend on

Table 2
Thickness of the layer of crust that has been removed by erosion

Age of crust	Mean age (Ga)	Minimum (km)	Average (km)	Maximum (km)
Archean	2.7	2.5	4.1	7.8
Early Proterozoic	2.1	1.65	2.53	4.4
Post-1.8 Ga	0.9	0.56	0.8	1.3

the fraction of trapped melt. We varied the depth of initial and final melting, and the mixture of melt and residual mantle to obtain the potential compositions of xenoliths containing trapped melt. The best-fit model for each xenolith sample was determined by a least-squares fit to a combination of three parameters that were determined to be most diagnostic: Al_2O_3 content, MgO/FeO, and CaO/Al_2O_3.

The best-fit models exhibit a fairly wide range of parameters, but they all require high mantle temperatures and therefore high degrees of melting (most greater than about 35%). Most of the models allow only small amounts of trapped melt, <4%. The average of the best-fit compositions for the South African xenoliths and the Lesotho xenoliths is given in Table 3.

The average of the best-fit models in both cases had a mantle potential temperature of 1900–1925°C, and a final depth of melting of 80–85 km. These conditions result in about 40% melting, with the best fits for individual xenoliths mostly between 35 and 45%. The compositions of the trapped melts formed under these conditions are high-Mg komatiites and are consistent with the primitive lava compositions of Archean komatiites, such as Belingwe.

For South Africa, the average composition of the depleted mantle resembles a peridotite that has been depleted by the extraction of 38.1% melt. The average amount of trapped melt in the best-fit model is 2.1% (Fig. 4). For Lesotho,. the average composition of the depleted mantle resembles a peridotite that has been depleted by the extraction of 40.0% melt. The best-fit model for Lesotho has an average of 1.7% trapped melt.

12. Checking our models of melting

We check that the melt does not represent unextracted melt rather than trapped melt by plotting Mg number of the xenolith versus our modeled per cent trapped melt. If the melt was simply unextracted primitive mantle, we would expect to see higher amounts of trapped melt in the xenoliths with the lowest Mg numbers. We do see a slight hint of such a trend, but Fig. 5 is an almost perfect scatter plot, consistent with our assertion that the xenoliths contain trapped melt rather than unextracted melt.

The compositions of the modeled trapped melt are extremely interesting. Both of the best-fit models of trapped melt have major element compositions that resemble those of komatiites (Table 3). The best-fit composition of both trapped melts resembles a Belingwe komatiite. Both of the trapped melt compositions are high in iron, with 10.8% FeO.

As a further check, we have calculated the mean composition of all xenoliths with an Mg number of less than 89, the Mg number of primitive undepleted mantle. These xenoliths must have high percentages of trapped melt. We find that their average composition is roughly komatiitic. The mean composition of the three xenoliths with the lowest Mg numbers is the most compelling. These

Table 3
Modeled composition of trapped melt and xenoliths plus trapped melt compared to the observed mean xenolith composition and the mean composition of xenoliths with Mg numbers less than 89

Rock type	SiO_2	CO	Al_2O_3	FeO	MgO
Mean South African xenoliths	46.5	1.2	1.6	6.6	44.1
Best-fit model South African xenoliths + melt	43.6	1.0	1.5	6.7	46.9
Trapped melt composition	47.4	7.5	7.3	10.8	27.0
Average all South African xenoliths with Mg# < 89	47.9 ± 2.3	4.9 ± 2.0	4.3 ± 0.89	10.1 ± 2.0	32.9 ± 3.5
Three lowest Mg # xenoliths (Mg# = 82.9)	46.8 ± 0.9	4.0 ± 0.8	4.6 ± 0.7	12.0 ± 0.7	32.6 ± 1.8
Mean lesotho xenoliths	46.4	0.8	0.9	6.4	45.6
Best-fit model Les. xenoliths + melt	43.6	0.9	1.3	6.6	48.2
Trapped melt composition	47.4	7.6	7.4	10.8	26.8

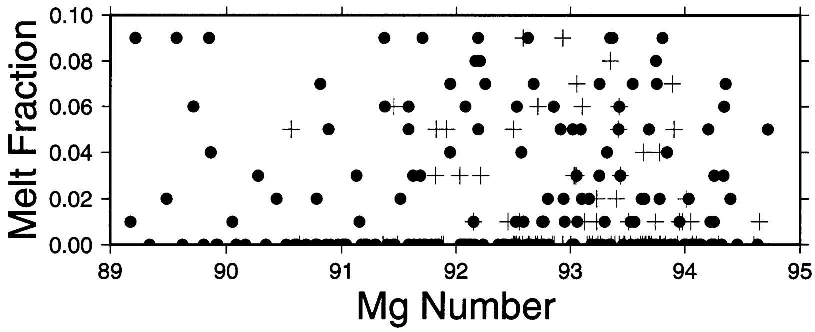

Fig. 5. Mg number of peridotites versus fraction of melt within the peridotite. Black dots: Archean peridotites. Crosses: Early Proterozoic peridotites. If the melt fraction represented unextracted melt, the plot would show a trend between melt fraction and Mg number. There is no trend, and the plot is an almost perfect scatter plot. This lack of a trend suggests that the melt fraction represents trapped melt rather than unextracted melt.

xenoliths have a composition that is clearly komatiitic and is very high in iron (Table 3).

We also estimate the reasonableness of these results by using the upper bound of the K_2O continent of the mantle root (Rudnick et al., 1998). Rudnick et al. (1998) estimated that mantle roots could have no more than 0.03% K_2O before the internal heat production would be too high to fit known crustal and cratonic geotherms. If we take the average K_2O content of lavas from the Ontong Java plateau ($0.326 \pm 0.02\%$) (Mahoney et al., 1992), a peridotite can have an average of 9.2% trapped melt before these limits are exceeded. This upper bound on the percentage of trapped melt is much higher than the percentages that we obtain.

If, however, we take a komatiitic trapped melt, the peridotite can have over 40% trapped melt before these limits on radiogenic heat production are exceeded. Because both of our model trapped melts were komatiitic, we conclude that our estimates for the percentage of trapped melt are reasonable for Early Proterozoic and Archean age lithospheric mantle. For younger lithosphere, we use the Early Proterozoic values of trapped melt (Table 4).

The amount of crust that is potentially trapped within the lithospheric mantle is significant.

Table 4
Volume of trapped melt within lithospheric mantle of different ages

Source	Melt minimum	Melt average	Melt maximum
South Africa	0.019	0.0211	0.0232
Lesotho	0.014	0.0166	0.0192
Rudnick (Ontong Java)	0.081	0.092	0.106
	Root minimum	Root average	Root maximum
Archean	197.1	203	208.9
Early Proterozoic	188.2	196	203.8
Post-1.8 Ga	93.3	97	100.7
	Crust minimum	Crust average	Crust maximum
Archean	3.74	4.28	4.85
Early Proterozoic	2.63	3.25	3.91
Post-1.8 Ga	1.31	1.61	1.93

Proportionately, Archean areas have the most trapped melt, equivalent to a crustal thickness of 3.7–4.9 km (Table 4). Early Proterozoic areas also have considerable amounts of trapped melt, equivalent to a crustal thickness of 2.6–3.9 km. For post-1.8 Ga crust, we estimate that the maximum amount of trapped melt is equivalent to an extra 1.3–1.9 km of crust. Thus, trapped melt may represent a significant portion of the crust extracted from the mantle, particularly in cratonic regions.

13. Constraining the rate of continental growth

The first technique, which we call the summation method, uses the sum of the following quantities to estimate the minimum volume of crust at different times in Earth history: distribution of crustal thickness, erosion level of the crust, and the amount of trapped melt. The surface areas are taken from our compilations of crustal ages. The crustal thicknesses are from the recent model of (Mooney et al., 1998). The amount of crust removed by erosion is taken from the work of Galer and Metzger (1998). Finally, we estimate the amount of unextracted melt in the lithospheric mantle using the compositions of mantle xenoliths. The amount of unextracted melt is multiplied by the total volume of the lithospheric root to derive an estimate of the amount of crust trapped within the lithospheric mantle. The sum of these three parameters, crustal thickness, crustal erosion, and trapped melt, equals the original amount of crust that was extracted from the mantle.

The second technique uses the corrected thickness of the continental lithosphere to estimate the overall crustal volume present at the end of the Archean, the Early Proterozoic and at the present time. Lithospheric roots are derived from partial melting of the mantle to make the crust. Thus, the overall thickness of the lithosphere of a given age is directly related to the amount of crust that was extracted from the mantle at that time in Earth history. Because the oldest Re/Os model ages either match or exceed the age of the oldest crust within a craton (Pearson et al., 1995a,b; Olive and Ellam, 1997; Graham et al., 1999), we believe that the root volume may be recycled much more slowly than the crustal volume. Thus, the lithospheric thickness may preserve a less biased record of the total amount of crust extracted from the mantle at a given time in the Earth's history.

14. Crustal extraction — the summation method

We computed the sum of the total amount of crust created for each of our three periods in Earth history. As shown in Table 5, after combining the seismic thickness, the eroded thickness, and the trapped melt, we found that the volume of crust produced in the Archean was considerable. If no melt had been trapped within the lithospheric mantle during the Archean, it would have been equivalent to an overall thickness of 43–55 km of crust. Similarly, when we included the melt that was trapped and frozen within the lithospheric mantle, Early Proterozoic crustal volume was equivalent to a crustal layer with a thickness of 39–57 km. The total equivalent thickness of post-Early Proterozoic crust was somewhat less, equivalent to a layer that is 32–47 km thick (Table 5).

As Table 5 shows, the summation method, which calculates the overall volume of crust that was extracted from the mantle, gives values for the volume of the continental crust over time that are much closer to the isotopic and geochemical estimates of total crustal volume (McLennan and Taylor, 1982; Taylor and McLennan, 1985; Veizer and Jansen, 1985; McCulloch and Bennett, 1994) than previous summations of crustal volume (Hurley and Rand, 1969). From the summation results, we estimate that at least 27–30% of the continental crust was extracted by the end of the Archean. By the end of the Early Proterozoic (1.8 Ga), between 50 and 52% of the continental crust had been extracted from the mantle (Fig. 5). However, the results of the summation method do not require large amounts of recycling of early formed continental crust.

15. Crustal volume through time — the melt column method

Our second method for estimating the volume of crust that was extracted relied on the overall

Table 5
Total thickness of crust through time derived from the summation method

	Minimum	Average	Maximum
Archean			
Seismic (km)	36.4	39.4	42.4
Eroded (km)	2.5	4.1	7.8
Melt (km)	3.7	4.3	4.8
Equivalent crustal thickness	42.6	47.8	55.1
Fraction trapped melt	0.0190	0.0211	0.0232
Root thickness (lith-crust)	197	203	209
Surface area (10^6 km^2)	36.8	40.9	45.0
Total volume (10^9 km^3)	1.6	2.0	2.5
Percentage total volume of all crust	29.9	28.2	27.5
Early Proterozoic			
Seismic (km)	35.0	41.6	48.3
Eroded (km)	1.7	2.5	4.4
Melt (km)	2.6	3.3	3.9
Equivalent crustal thickness	39.2	47.4	56.6
Fraction trapped melt	0.0140	0.0166	0.0192
Root thickness (lith-crust)	188	196	204
Surface area (10^6 km^2)	29.3	32.5	35.7
Total volume (10^9 km^3)	1.1	1.5	2.0
Percentage total volume of all crust	21.9	22.2	22.4
Post-1.8 Ga			
Seismic (km)	30.3	37.1	43.9
Eroded (km)	0.6	0.8	1.3
Melt (km)	1.3	1.6	1.9
Equivalent crustal thickness	32.2	39.5	47.1
Fraction trapped melt	0.0140	0.0166	0.0192
Root thickness (lith-crust)	93	97	101
Surface area (10^6 km^2)	78.4	87.1	95.8
Total volume (10^9 km^3)	2.5	3.4	4.5
Percentage total volume of all crust	48.1	49.6	50.1
All crust			
Total volume (10^9 km^3)	5.2	6.9	9.0

thickness of the lithospheric mantle and theoretical modeling of melt extraction. We assumed that present-day lithospheric thickness, after a correction for erosion, provided a valid estimate of the depth at which melt began to be extracted to make the crust. We then used models based on experimental results to estimate the amount of melt that would have been extracted. This value was multiplied by the thickness of the depleted lithospheric root to obtain an estimate of the amount of crust that had been extracted by a given time in Earth history. The results of these calculations are shown in Tables 6 and 7 and in Fig. 6.

16. Checking our melt column results using average xenolith composition

A check on the melt column method of estimating the volume of crustal extraction is based on theoretical models of xenolith composition. These models are the same models that were used to estimate the amount of trapped, congealed melt using xenolith suites from South Africa and Lesotho. Because mantle xenoliths sample only the uppermost part of the lithospheric root, the average degree of melting represented by the xenolith suite is larger than the average degree of melting within the lithospheric root.

Table 6
Total thickness of crust through time derived from the melt column method

	Minimum	Average	Maximum
Archean			
Seismic (km)	36.4	39.4	42.4
Eroded (km)	2.5	4.1	7.8
Root thickness (km)	197	203	209
Present lithospheric thickness (km)	236	247	259
Past lithospheric thickness (km)	238	251	267
Surface area (10^6 km^2)	36.8	40.9	45.0
Average fraction melted (melt column)	0.300	0.317	0.337
Average fraction melted (xenolith composition)	0.311	0.381	0.451
Average fraction melted (upper 160 km)	0.344	0.381	0.423
Crustal thickness (km) (melt column)	59.1	64.4	70.4
Crustal volume (10^9 km^3) (melt column)	2.2	2.6	3.2
Percentage total volume (melt column)	46.3	45.1	44.1
Early Proterozoic			
Seismic (km)	35.0	41.6	48.3
Eroded (km)	1.7	2.5	4.4
Root thickness (km)	188	196	204
Present lithospheric thickness (km)	225	240	256
Past lithospheric thickness (km)	226	243	261
Surface area (10^6 km^2)	29.3	32.5	35.7
Average fraction melted (melt column)	0.284	0.306	0.330
Average fraction melted (xenolith composition)	0.350	0.400	0.450
Average fraction melted (upper 160 km)	0.313	0.359	0.407
Crustal thickness (km) (melt column)	53.4	60.0	67.3
Crustal volume (10^9 km^3) (melt column)	1.6	1.9	2.4
Percentage total volume (melt column)	33.3	33.4	33.4
Post-1.8 Ga			
Seismic (km)	30.3	37.1	43.9
Eroded (km)	0.6	0.8	1.3
Root thickness (km)	93	97	101
Present lithospheric thickness (km)	124	135	146
Past lithospheric thickness (km)	125	136	147
Surface area (10^6 km^2)	78.4	87.1	95.8
Average fraction melted (melt column)	0.131	0.149	0.167
Crustal thickness (km) (melt column)	12.2	14.5	16.8
Crustal volume (10^9 km^3) (melt column)	1.0	1.3	1.6
Percentage total volume (melt column)	20.4	21.6	22.4
All crust			
Crustal volume (10^9 km^3) (melt column)	4.7	5.8	7.2

We model the average degree of melting in the xenoliths, assuming that the overall lithospheric thickness is the same as our estimated past lithospheric thickness, but that the xenoliths sample only the upper 160 km of the melt column. This value of 160 km is based on a maximum depth of origin of the xenoliths of about 200 km (Finnerty and Boyd, 1987; Pearson et al., 1995a,b) and assumes a 40 km thick crust. We call this a truncated melt column model. The truncated melt column model of the average fraction of melting in the xenoliths matches our theoretical estimates of the average fraction of melting in the xenoliths (Table 6). We take this as a confirmation that our

Table 7
Comparison of the cumulative volume of continental crust extracted through time from the melt column and summation methods

Age	Percentage total crust	Error
Method 1: Trapped melt + erosion + seismic		
2.7	28.7	1.2
2.1	50.9	0.9
0	100.0	0.3
Method 2: Melt column		
2.7	45.2	1.1
2.1	78.6	1.1
0	100.0	4.8

seismic estimate of the overall length of the melt column is basically correct.

17. Volume of crust from xenolith composition and melt column models

The average fraction of melting in the melt column is multiplied by the thickness of the depleted lithospheric root to obtain the amount of crust extracted by a given time in Earth history (Table 6, Fig. 5). From the melt column model, we obtain an equivalent of 59–70 km of crust extracted from the mantle by the end of the

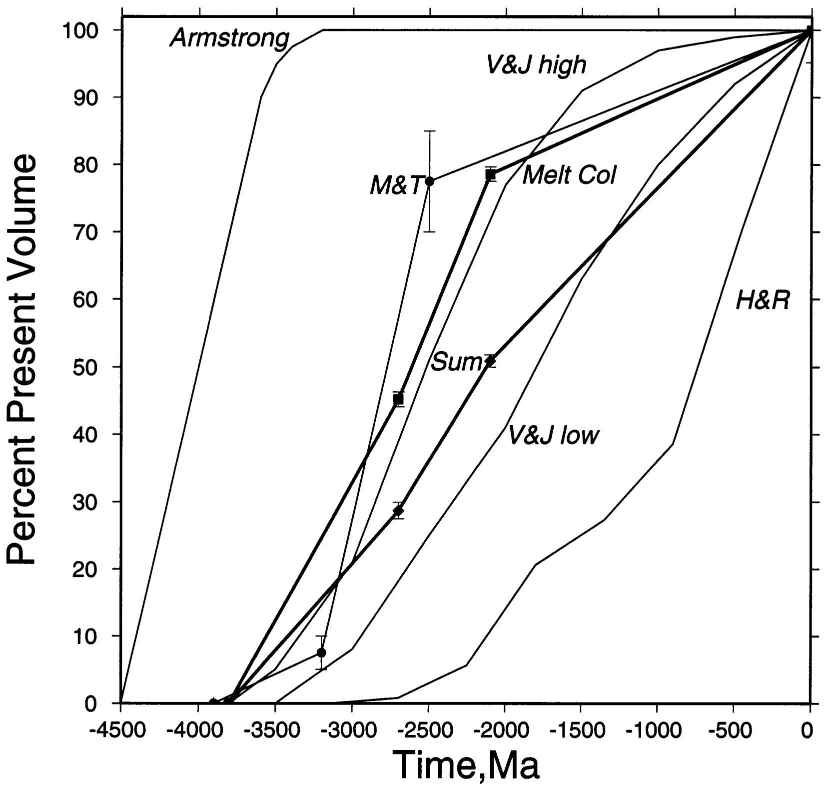

Fig. 6. Cumulative volume of continental crust extracted through time from the two methods compared to some other models of the volume of continental crust extracted through time. In order to keep the figure legible, the models are not exhaustive. H&R: Hurley and Rand (1969); M&T: McLennan and Taylor (1982); V&J: Veizer and Jansen (1985); Armstrong: Armstrong (1981). Sum: our results from summing the overall volume of the seismic crust, eroded crust, and trapped melt in the lithospheric mantle. Melt Col: Our results from assuming that the lithospheric root is the residue of a melt column. Thus, the overall lithospheric thickness is an estimate of where melting starts. This type of melting model is consistent with the average amount of melting within mantle xenoliths from Archean and Early Proterozoic age mantle roots. Note that our estimate of crustal volume through time does not include the areas north and south of 80°.

Archean. For Early Proterozoic time, the equivalent thickness of crust is between 53 and 67 km. For post-Early Proterozoic time, the equivalent thickness of crust is only 12–17 km.

When we consider the distribution of crustal extraction over time from the melt column models, we obtain a crustal growth history that closely approaches the estimates of McLennan and Taylor (1982). Overall, the melt column results imply that a minimum of 44–46% of continental crust was extracted by the end of the Archean. By the end of the Early Proterozoic (1.8 Ga), between 77 and 79% of the continental crust was extracted from the mantle (Fig. 6).

18. Discussion: crustal thicknesses and volumes

The melt column models of melt extraction predict that large amounts of crust were extracted from the lithospheric mantle in the Archean and Early Proterozoic. For pre-1.8 Ga, the composite crustal thicknesses from the melt column models are much larger than those from the summation method. However, the melt column results for post-1.8 Ga crust are much smaller than the results from the summation method. The experimentally based models of melt extraction predict that only about 15 ± 2 km of crust has been extracted from the mantle in areas of post-1.8 Ga crust (Table 6). This number contrasts quite markedly with the estimated crustal thickness of post-1.8 Ga crust from seismic observations, estimated erosion, and estimated trapped melt fraction, which averages about 40 km (Table 5).

There are several possible explanations for this discrepancy. Some workers have found that the seismic thickness overestimates the true geochemical crustal thickness in areas of high heat flow (Griffin and O'Reilly, 1987). However, the continental areas of high heat flow are relatively spatially restricted, and thus, this cannot explain the overall pattern.

The second possibility is that the use of the metamorphic grade of undeformed Archean greenstone belts to estimate the degree of erosion of the crust underestimates the true amount of crustal erosion since 3.0 Ga. By picking undeformed greenstone belts, we are, by definition, excluding greenstone belts that have had no erosion due to tectonic compression. We know that large areas of the Earth's crust have undergone tectonic compression since the crust was initially extracted from the mantle. Recent work also suggests that some greenstone belts represent thrust slices of the upper few kilometers of Archean oceanic plateaus (Kusky and Kidd, 1992; Kusky and Vearncombe, 1997). If this is generally true of undeformed greenstone belts, this means that undeformed greenstone belts record only the erosion that occurred after their emplacement. Therefore, we need some other complementary method of estimating the amount of erosion experienced by the continental crust through time.

A third problem is that we know that not all depleted mantle is sufficiently buoyant to resist subduction. As a result, the basal part of the melt column that melts to form the continental crust is reincorporated into the convecting mantle. Unfortunately, we do not really know exactly how much of the basal part of the melt column is remixed into the mantle. We do know that some depleted mantle is remixed: this is the origin of the depleted mantle signature of MORB (mid-ocean ridge basalts). Consequently, our estimates of melt extraction from experimental data combined with the overall thickness of the lithospheric root can only be minimum values.

Finally, there is the possibility that these differences in the estimated amount of crustal extraction are basically a reflection of the relative importance of recycling and new crustal extraction. In that case, the difference in estimated crustal thickness derived from lithospheric thickness and observed seismic thickness is an estimate of the difference between the amount of new crustal extraction and the amount of recycled continental crust. This is a reasonable inference because our estimates of the rate of crustal growth from experimental constraints and lithospheric thickness are much closer to geochemical models than any previous, geophysically based mass-balance calculations.

19. Importance of the trapped melt

The theoretically based estimates of the amount and composition of trapped melt suggest that the continental lithospheric mantle contains large quantities of iron-rich, komatiitic melt, which, according to our models, has an average FeO content of about 10.8%. This result is important because it can help to explain the discrepancy between the FeO content of lower crustal xenoliths within Archean cratons (about 9%) and the known FeO content of komatiitic melts. Furthermore, it has been suggested that melting of a primitive, previously unmelted mantle would produce high degree melts with an average FeO content of 9% (O'Neill and Palme, 1988). As a result, there is no need for a mechanism to delaminate the lower crust in Archean times. These ideas are much more compatible with the evidence that thick Archean continental lithosphere formed very quickly and cooled very rapidly (Nisbet, 1987; Abbott, 1991; Pearson et al., 1995a)

Overall, our estimates of volumes of trapped melt within Archean and Early Proterozoic cratonic roots indicate that much of the komatiitic melt that was generated within the mantle was trapped within the root. Only relatively small proportions made it to the surface. The residual melt that did reach the surface was, in most cases, basaltic, with much less iron. This can also explain why komatiites are so rare in greenstone belts, constituting at most a few per cent of the overall volume of extrusive rocks (de Wit and Ashwal, 1997) .

This model of the origin of the moderate iron content of lower continental crust is testable in several ways. This model suggests that the iron content of oceanic plateau basalts may be higher in shallower layers than in deeper layers of the crust. This inference can be tested by looking at crustal xenolith suites within oceanic plateaus that are too young to be modified by arc volcanism. The xenolith localities on the island of Malaita in the Solomons tap the lithosphere of the Ontong Java Plateau. If the crustal xenoliths could be characterized by FeO content and depth of origin, they would constitute an important test of this model.

The melt column model of crustal extraction also suggests that areas of thick lithospheric mantle are dominantly very old. In some cases, there are proposed areas of thick lithosphere that lie entirely within the ocean basins. One notable candidate is the Mascarene bank, south of Madagascar (Fig. 3a). If Madagascar is returned to its former position in north Africa, this proposed area of thick lithosphere lies next to the Zimbabwe and Kaapvaal cratons. This supposition about a thick lithosphere could be tested by a seismic experiment with stations on Reunion, Madagascar and South Africa. Other areas where this assumption could be tested include the Seychelles and the Ogasawara plateau.

20. Conclusions

The results of a geophysically based compilation of the volume of continental crust generated through time are most consistent with isotopic and geochemical studies that indicate that relatively large volumes of continental crust were extracted early in Earth's history (McLennan and Taylor, 1982; Taylor and McLennan, 1985; Veizer and Jansen, 1985; Calderwood, 1998; McCulloch and Bennett, 1998; Sylvester, 1998). Although our present results do not match the models with the greatest amount of early extraction, our technique is biased towards younger ages of crustal extraction by the selection of 2.4 Ga as our first age interval. Our technique is also biased towards smaller lithospheric thicknesses in areas of Archean basement by the smearing effects of the tomographic model. As a result, it is likely that a better tomographic model combined with smaller age divisions would produce higher estimates of the amount of early crustal growth.

We suggest that the greater lithospheric thickness of Archean cratons is a direct result of the large amounts of crust extracted during that era. Some of this crust never made it to the surface, but was stored as congealed trapped melt within the lithospheric mantle. This trapped melt is quite komatiitic in mean composition, meaning that it is rich in iron. In addition, melting of previously undepleted mantle may produce melts that are lower in iron than melts of mantle containing recycled crustal material. Thus, the low iron content of Archean crust is not the result of lithospheric delamination, but rather the result of sequestration of iron within Archean lithospheric roots and the result of deriving continental crust from melting within a truly primitive mantle.

The discrepancies between the volumes of crust inferred from melt column models and xenolith composition models and those inferred from summations of the geophysical crust, eroded crust, and trapped melt volumes are partially the result of a transfer of mass by recycling (Veizer and Jansen, 1985). Within Archean and Proterozoic cratons, the equivalent thickness of crust from the summation method is less than the equivalent thickness of crust from the melt column method. We suggest that these differences reflect the lateral transfer of mass from Archean cratons to Proterozoic cratons by erosion and recycling within subduction zones.

Our studies also suggest that there are some areas of unrecognized cratonic basement that lie within the ocean basins. In some cases, the cratonic basement has been rifted off from other cratons and is covered by volcanic rocks (e.g. the Mascarene bank, the Ogasawara plateau) (Ishii, 1985; Bassias et al., 1993). However, these volcanic rocks may retain a cratonic signature within their isotopes, in particular in Re/Os. The chemistry of these volcanic rocks should be studied with this hypothesis in mind. Once we have a full inventory of the areas of Archean and Early Proterozoic age cratonic roots, we will be able to make a more accurate assessment of the amount of early crustal growth.

Acknowledgements

We thank Martin Menzies, Stephen Galer, and Steve Grand for helpful, constructive reviews of the manuscript. D. Sparks thanks NSF contract #EAR-9614178 for support of this work. LDEO contribution number 6064.

References

Abbott, D.H., Hoffman, S.E., 1984. Archean plate tectonics revisited 1: Heat flow, spreading rate, and the age of subducting oceanic lithosphere and their effects on the origin and evolution of continents. Tectonics 3, 429–448.

Abbott, D.H., 1991. The case for accretion of the tectosphere by buoyant subduction. Geophys. Res. Lett. 18, 585–588.

Abbott, D., Burgess, L., Longhi, J., Smith, W.H.F., 1994. An empirical thermal history of the Earth's upper mantle. J. Geophys. Res. 99, 13 835–13 850.

Abbott, D.H., Mooney, W.D., 1995. Crustal Structure and Evolution: Support for the Oceanic Plateau Model of Continental Growth. Reviews of Geophysics, Supplement, US National Report to the IUGG. pp. 231–242

Abbott, D.H., Drury, R., Mooney, W., 1997. Continents as lithological icebergs: the importance of buoyant lithospheric roots. Earth Planet. Sci. Lett. 149, 15–27.

Abouchami, W., Boher, M., Michard, A., Albarede, F., 1990. A major 2.1 Ga event of mafic magmatism in West Africa: an early stage of crustal accretion. J. Geophys. Res. 95, 17 605–17 629.

Agee, C.B., Walker, D., 1993. Olivine flotation in mantle melt. Earth Planet. Sci. Lett. 114, 315–324.

Agrawal, P.K., Pandey, O.P., Negi, J.G., 1992. Madagascar: A continental fragment of the paleo-super Dharwar craton of India. Geology 20, 543–546.

Armstrong, R.L., 1981. Radiogenic isotopes: the case for crustal recycling on a near-steady-state no-continental growth Earth. Philos. Trans. R. Soc. London Ser. A 301, 443–472.

Bardet, M.G., 1973. Geologie du diamont: Paris — France. Bureau de Recherches Geologiques et Minieres, Paris.

Bardet, M.G., 1974. Geologie du diamant: deuxieme partie: Gisements de diamant d'Afrique: Paris — France. Bureau de Recherches Geologiques et Minieres, Paris.

Bassias, Y., Denis-Clocchiatti, M., Leclaire, L., 1993. Le Plateau des Mascareignes, evolution d'une plate-forme neritique en mileau oceanique. C. R. Acad. Sci. 317, 507–514.

Boher, M., Abouchami, W., Michard, A., Albarede, F., Arndt, N.T., 1992. Crustal growth in West Africa at 2.1 Ga. J. Geophys. Res. 97, 345–369.

Boyd, F.R., 1987. High and low temperature garnet peridotite xenoliths and their possible relation to the lithosphere–asthenosphere boundary beneath southern Africa. In: Nixon, P.H. (Ed.), Mantle Xenoliths. Wiley, Chichester, UK, pp. 403–412.

Calderwood, A.R., 1998. Sm–Nd isotopic modeling of the evolution of the Earth's depleted mantle and crust, estimates of continental recycling and accretion rates. Geol. Soc. Am. Abstr. Programs, 30, 207

Christensen, N.I., Mooney, W.D., 1995. Seismic velocity structure and composition of the continental crust: a global view. J. Geophys. Res. 100, 9761–9788.

Condie, K.C., 1999. Mafic crustal xenoliths and the origin of lower continental crust. Lithos 46, 95–102.

de Wit, M.J., Armstrong, R., 1987. Felsic igneous rocks within the 3.3 to 3.5-Ga Barberton Greenstone Belt: High crustal level equivalents of the surrounding tonalite–trondhjemite terrain, emplaced during thrusting. Tectonics 6 (5), 529–549.

de Wit, M.J., Jones, M.G., Buchanan, D.L., 1992. The geology and tectonic evolution of the Pietersburg Greenstone Belt, South Africa. Precambrian Res. 1, 123–153.

de Wit, M.J., Ashwal, L.D., 1997. Greenstone Belts. Clarendon Press, Oxford.

Durrheim, R.J., Mooney, W.D., 1991. Archean and Proterozoic crustal evolution: evidence from crustal seismology. Geology 19, 606–609.

Eggler, D., Furlong, K.P., 1991. Destruction of subcratonic mantle keel: the Wyoming Province. Fifth International Kimberlite Conference, Extended Abstracts, Araxa, Brazil, United States.

Finnerty, A.A., Boyd, F.R., 1987. Thermobarometry for garnet peridotites: basis for the determination of thermal and compositional structure of the upper mantle. In: Nixon, P.H. (Ed.), Mantle Xenoliths. Wiley, Chichester, UK, pp. 381–402.

Galer, S.J.G., 1991. Interrelationships between continental freeboard, tectonics and mantle temperatures. Earth Planet. Sci. Lett. 105, 214–228.

Galer, S.J.G., Metzger, K., 1998. Metamorphism, denudation and sea level in the Archean and cooling of the Earth. Precambrian Res. 92, 389–412.

Gossler, J., Kind, R., 1996. Seismic evidence for very deep roots of continents. Earth Planet. Sci. Lett. 138, 1–13.

Graham, S., Lambert, D.D., Shee, S.R., Smith, C.B., Reeves, S., 1999. Re–Os isotopic evidence for Archean lithospheric mantle beneath the Kimberly block — Western Australia. Geology 27, 385–480.

Grand, S., 1986. Shear Velocity Structure of the Mantle Beneath the North American Plate. California Institute of Technology.

Griffin, W.L., O'Reilly, S.Y., 1987. The composition of the lower crust and the nature of the continental Moho — xenolith evidence. In: Nixon, P.H. (Ed.), Mantle Xenoliths. Wiley, Chichester, UK, pp. 413–432.

Griffin, W.L., et al., 1999. Layered mantle lithosphere in the Lac de Gras area, Slave craton, Composition, structure and origin. J. Petrol. 40, 727–795.

Gurnis, M., Davies, G.F., 1986. Apparent episodic crustal growth arising from a smoothly evolving mantle. Geology 14, 396–399.

Handke, M.J., Tucker, R.D., Hamilton, M.A., 1997. Early Neoproterozoic (800–790 Ma) intrusive rocks in central Madagascar, geochemistry and petrogenesis. Geol. Soc. Am., Abstr. Programs 29, 468.

Herzberg, C.T., Fyfe, W.S., Carr, M.J., 1983. Density contraints on the formation of the continental Moho and crust. Contrib. Mineral. Petrol. 84, 1–5.

Herzberg, C., 1999. Phase equilibrium constraints on the formation of cratonic mantle. Mantle petrology: field observations and high pressure experimentation: A tribute to Francis R. (Joe) Boyd. In: Fei, Y., Bertka, C., Mysen, B.O. (Eds.), Geochemical Society Spec. Publ. 6, 241–257.

Herzberg, C., Hara, M.J.O., 1998. Phase equilibrium constraints on the origin of basalts, picrites, and komatiites. Earth-Sci. Rev. 44, 39–79.

Hurley, P.M., Rand, J.M., 1969. Pre-drift continental nuclei. Science 164, 1229–1242.

Ireland, T.R., Rudnick, R.L., Spetsius, Z., 1994. Trace elements in diamond inclusions from eclogites reveal link to Archean granites. Earth Planet. Sci. Lett. 128, 199–213.

Ishii, T., 1985. Dredged samples from the Osagawara fore-arc seamount or 'Osagawara Paleoland'–'fore-arc ophiolite'. In: Nasu, N., et al. (Eds.), Formation of Active Ocean Margins, pp. 307–342.

Jordan, T.H., 1978. Composition and development of the continental tectosphere. Nature 274, 544–548.

Jordan, T.H., 1988. Structure and formation of the continental tectosphere. Special Lithosphere Issue. J. Petrol., 11–37.

Kay, R.W., Kay, S.M., 1986. Petrology and geochemistry of the lower continental crust: an overview. In: Dawson, J.B., Carswell, D.A., Hall, J., Wedepohl, K.H. (Eds.), The Nature of the Lower Continental Crust, pp. 147–159.

Kennedy, C.S., Kennedy, G.C., 1969. The equilibrium boundary between graphite and diamond. J. Geophys. Res. 81, 2467–2470.

Kusky, T.M., Kidd, W.S.F., 1992. Remnants of an Archean oceanic plateau, Belingwe greenstone belt, Zimbabwe. Geology 20, 43–46.

Kusky, T.M., Vearncombe, J.R., 1997. Structure of Archean greenstone belts. Tectonic evolution of greenstone belts. In: de Wit, M., Ashwal, L.D. (Eds.), Greenstone Belts. Clarendon Press, Oxford, pp. 91–124.

Lambert, D.D., Shirey, S.B., Shirey, S.C., 1995. Proterozoic lithospheric mantle source for the Prairie creek lamproites: Re–Os and Sm–Nd isotopic evidence. Geology 23, 273–276.

Larson, R.L., 1991. Geological consequences of superplumes. Geology 19, 963–966.

Lerner-Lam, A.L., Jordan, T.H., 1987. How thick are the continents? J. Geophys. Res. 92, 14 007–14 040.

Liu, M., 1994. Asymmetric phase effects and mantle convection patterns. Science 264, 904–1907.

McCulloch, M.T., Bennett, V.C., 1994. Progressive growth of the Earth's continental crust and depleted mantle: Geochemical constraints. Geochim. Cosmochim. Acta 58, 4717–4738.

McCulloch, M.T., Bennett, V.C., 1998. Early Differentiation of the Earth: An Isotopic Perspective. In: Jackson, I. (Ed.), The Earth's Mantle. Cambridge University Press, Cambridge, pp. 127–158.

McLennan, S.M., Taylor, S.R., 1982. Geochemical constraints on the growth of the continental crust. J. Geol. 90, 347–361.

Mahoney, J.J., Storey, M., Duncan, R.A., Spencer, K.J., Pringle, M., 1992. Geochemistry and geochronology of leg 130 basement lavas: Nature and origin of the Ontong Java plateau. In: Berger, W.H., Kroenke, L.W., Mayer, L.A. (Eds.), Proceedings of the Ocean Drill. Progr. Sci. Results. College Station, TX, Ocean Drilling Program, 3–22.

Mann, P., Gahagan, L., Coffin, M., Shipley, T., Cowley, S., Phinney, E., 1997. Regional tectonic effects resulting from the progressive east-to-west collision of the Ontong Java Plateau with the Melanesian Arc system. EOS Trans. Am. Geophys. Union 77, 712

Martin, H., 1986. Effect of steeper Archean geothermal gradient on geochemistry of subduction-zone magmas. Geology 14, 753–756.

Menke, W., Levin, V., 1994. Cold crust in a hot spot. Geophys. Res. Lett. 21, 1967–1970.

Menzies, M.A., Zhang, M., Weiming, F., 1993. Paleozoic and Cenozoic lithoprobes and the loss of >120k of Archean Lithosphere from the Sino-Korean craton China. In: Pritchard, H. (Ed.), Magmatic Processes and Plate Tectonics. Geological Society of London, London, pp. 71–81.

Menzies, M.A., Xu, Y., Flower, M.F.J., Chung, S.L., Lo, H., Lee, T.Y., 1998. Geodynamics of the North China Craton. In: Chung, S.L., Lo, C.H., Lee, T.Y. (Eds.), Mantle Dynamics and Plate Interactions in East Asia. American Geophysical Union, Washington, DC, pp. 155–165.

Mooney, W.D., Laske, G., Masters, T.G., 1998. Crust 5.1, a global crustal model at 5 by 5 degrees square. J. Geophys. Res. 103, 727–747.

Nisbet, E.G., 1987. The Young Earth: An Introduction to Archean Geology. Allen and Unwin, Boston, MA.

Nixon, P.H., 1987. Mantle Xenoliths. Wiley, Chichester, UK.

Nolet, G., Grand, S.P., Kennett, B.L.N., 1994. Seismic heterogeneity in the upper mantle. J. Geophys. Res. 99, 23 753–23 766.

Nyblade, A.A., Pollack, H.N., 1993. A global analysis of heat flow from Precambrian terrains: Implications for the thermal structure of Archean and Proterozoic lithosphere. J. Geophys. Res. 98, 12 207–12 218.

Ohtani, E., Nagata, Y., Suzuki, A., Kato, T., 1995. Melting relations of peridotite and the density crossover in planetary mantles. In: McDonough, W.F., Arndt, N.T., Shirey, S. (Eds.), Chemical Evolution of the Mantle. Elsevier, Amsterdam, pp. 207–221.

Olive, V., Ellam, R.M., 1997. A Re–Os isotope study of ultramafic xenoliths from the Matsoku kimberlite. Earth Planet. Sci. Lett. 150, 129–140.

O'Neill, S.C., Palme, H., 1988. Composition of the silicate Earth: implications for accretion and core formation. In: Jackson, I. (Ed.), The Earth's Mantle: Composition Structure and Evolution. Cambridge University Press, Cambridge, pp. 3–126.

Parkinson, I.J., Hawkesworth, C.J., Cohen, A.S., 1998. Ancient mantle in a modern arc: Osmium isotopes in Izu–Bonin–Mariana forearc peridotites. Science 281, 2011–2013.

Pearce, J.A., et al., 1992. Boninite and harzburgite from Leg 125 (Bonin–Mariana forearc): A case study of magma genesis during the initial stages of subduction. In: Fryer, P., Pearce, J.A., Stokking, L.B. (Eds.), Proc. Ocean Drill. Progr. Sci. Results. National Science Foundation, Washington, DC, pp. 623–659.

Pearson, D.G., Carlson, R.W., Shirey, S.B., Boyd, F.R., Nixon, P.H., 1995a. Stabilization of Archean lithospheric mantle: a Re–Os isotope study of peridotite xenoliths from the Kaapvaal craton. Earth Planet. Sci. Lett. 134, 341–357.

Pearson, D.G., Shirey, S.B., Carlson, R.W., Boyd, F.R., Pokhilenko, N.P., Shimuzu, N., 1995b. Re–Os, Sm–Nd, and Rb–Sr isotopic evidence for thick Archean lithospheric mantle beneath the Siberian craton modified by multistage metasomatism. Geochim. Cosmochim. Acta 59, 959–977.

Petterson, M.G., et al., 1997. Structure and deformation of north and central Malaita, Solomon Islands: tectonic implications for the Ontong Java Plateau–Solomon arc collision, and for the fate of oceanic plateaus. Tectonophysics 283, 1–33.

Plank, T., Langmuir, C.W., 1988. An evaluation of the global variations in the major element chemistry of arc basalts. Earth Planet. Sci. Lett. 90, 349–370.

Rambelson, R.A., 1998. The Malagasy Shield. In: de Wit, M., Ashwal, L.D. (Eds.), Greenstone Belts. Clarendon Press, Oxford, pp. 636–639.

Revenaugh, J., Jordan, T.H., 1991. Mantle layering from ScS reverberations: 2, the transition zone. J. Geophys. Res. 96, 19 763–19 780.

Reymer, A., Schubert, G., 1986. Rapid growth of some major segments of continental crust. Geology 14, 299–302.

Richter, F.M., 1988. A major change in the thermal state of the Earth at the Archean Proterozoic boundary: consequences for the nature and preservation of continental lithosphere. Special Lithosphere Issue. J. Petrol. 1, 39–52.

Riganti, A., Wilson, A.H., 1995. Geochemistry of the mafic/ultramafic volcanic associations of the Nondweni greenstone belt, South Africa, and constraints on their petrogenesis. Lithos 34, 235–252.

Rudnick, R., Presper, T., 1990. Geochemistry of intermediate to high pressure granulites. In: Vielzeuf, D., Vidal, P. (Eds.), Granulites and Crustal Differentiation. Kluwer, Amsterdam, pp. 523–550.

Rudnick, R.L., 1992. Xenoliths — Samples of the lower continental crust. In: Fountain, D., Arculus, R., Kay, R.W. (Eds.), Continental Lower Crust. Elsevier, New York, pp. 269–316.

Rudnick, R., 1995. Making Continental Crust. Nature 378, 571–578.

Rudnick, R.L., Fountain, D.M., 1995. Nature and composition of the continental crust: a lower crustal perspective. Rev. Geophys. 33, 267–309.

Rudnick, R.L., McDonough, W.P., O'Connell, R.J., 1998. Thermal structure, thickness, and composition of continental lithosphere. Chem. Geol. 145, 395–411.

Smoot, N.C., Richardson, D.B., 1988. Tectonic and geomorphic interpretation of the Osagawara Plateau by multibeam-based 3D methods. Mar. Geol. 79, 141–147.

Stein, M., Hofmann, A.W., 1994. Mantle plumes and episodic crustal growth. Nature 372, 63–68.

Stein, M., Goldstein, S.L., 1996. From plume head to continental lithosphere in the Arabian Nubian Shield. Nature 382, 773–777.

Stoddard, P.R., Abbott, D.H., 1996. The influence of the tectosphere upon plate motion. J. Geophys. Res. 101, 5425–5433.

Sylvester, P.J., 1998. Formation of the continents, dribble or big bang? The Geochemical News 94, 12–25.

Taylor, S.R., McLennan, S.M., 1985. The Continental Crust: Its Composition and Evolution. Blackwell Scientific, Oxford.

Tucker, R.D., Ashwal, L.J., Handke, J., Hamilton, M.A., LeGrange, M., Rambleson, R.A., 1999. U–Pb geochronology and isotope geochemistry of the Archean and Proterozoic gneiss belts of Madagascar. J. Geol. 107, 135–154.

Veizer, J., Jansen, S.L., 1985. Basement and sedimentary recycling — 2: time dimension to global tectonics. J. Geol. 93 (6), 625–643.

Wasserburg, G.J., MacDonald, G.J., Hoyle, F., Fowler, W.A., 1964. Relative contributions of uranium, thorium, and potassium to heat production in the Earth. Science 143, 465.

Wyman, D.A., 1999. Paleoproterozoic boninites in an ophiolite-like setting. Geology 27, 455–458.

Yanagi, T., Wakizaka, Y., Suwa, K., 1983. Rb–Sr whole rock ages of granitic rocks from the Seychelles Islands. In: Eighth Preliminary Report of African Studies. University of Nagoya, Nagoya, pp. 23–26.

Zhang, Y.S., Tanimoto, T., 1991. Global love wave phase velocity variation and its significance to plate tectonics. Phys. Earth Planet. Inter. 66, 160–202.